

DepthFlow: Exploiting Depth-Flow Structural Correlations for Unsupervised Video Object Segmentation

Suhwan Cho¹ Minhyeok Lee² Jungho Lee² Donghyeong Kim² Sangyoun Lee²

¹ GenGenAI ² Yonsei University

<https://github.com/suhwan-cho/DepthFlow>

Abstract

Unsupervised video object segmentation (VOS) aims to detect the most prominent object in a video. Recently, two-stream approaches that leverage both RGB images and optical flow have gained significant attention, but their performance is fundamentally constrained by the scarcity of training data. To address this, we propose DepthFlow, a novel data generation method that synthesizes optical flow from single images. Our approach is driven by the key insight that VOS models depend more on structural information embedded in flow maps than on their geometric accuracy, and that this structure is highly correlated with depth. We first estimate a depth map from a source image and then convert it into a synthetic flow field that preserves essential structural cues. This process enables the transformation of large-scale image-mask pairs into image-flow-mask training pairs, dramatically expanding the data available for network training. By training a simple encoder-decoder architecture with our synthesized data, we achieve new state-of-the-art performance on all public VOS benchmarks, demonstrating a scalable and effective solution to the data scarcity problem.

1. Introduction

Video object segmentation (VOS) is a fundamental task in computer vision, playing a crucial role in various applications. Depending on the use case, VOS may incorporate external guidance such as initial frame masks, points, human interaction, or language expressions. This study focuses on the unsupervised setting, where the goal is to segment the most salient object without any external guidance.

In unsupervised VOS, also referred to as video salient object detection (SOD), two-stream approaches have recently gained considerable attention. These methods typically extract optical flow maps between adjacent frames using optical flow estimation models, then leverage image-flow pairs as inputs to generate segmentation masks. Con-

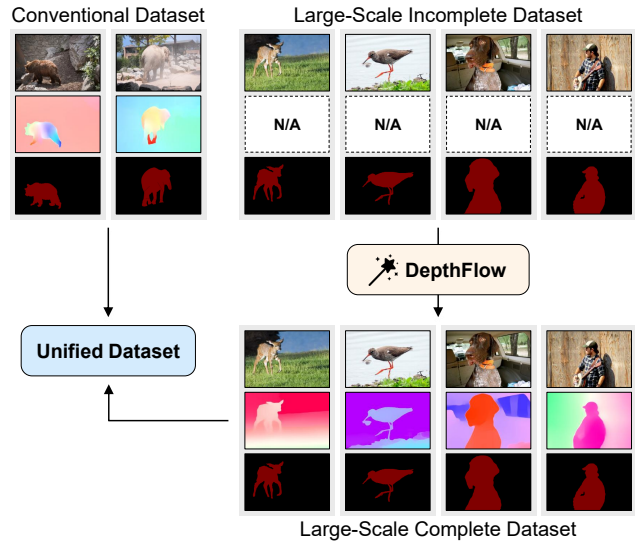


Figure 1. Overview of our synthetic data generation approach. We convert estimated depth maps from single images into plausible optical flows, creating large-scale image-flow-mask training pairs.

sequently, network training requires complete datasets comprising RGB images, optical flow maps, and segmentation masks. However, their performance is fundamentally constrained by the scarcity of such complete datasets, which remains a significant bottleneck.

Existing methods attempt to address this challenge by leveraging large-scale incomplete datasets, such as general video segmentation datasets [8, 9, 51] or image-level SOD datasets [3, 37, 44]. However, video segmentation datasets often include masks unsuitable for unsupervised VOS (e.g., non-salient objects), while image-level SOD datasets lack optical flow maps, limiting their effectiveness as primary training sources. Consequently, fine-tuning on small-scale complete datasets becomes necessary but remains insufficient for robust model training.

To address this, we propose DepthFlow, a novel data generation method that synthesizes optical flow from single

images. Our approach is based on the key insight that VOS models rely on the structural information in flow maps, not their geometric precision, and that this structure is highly correlated with depth. We first estimate a depth map from a source image and then convert it into a synthetic flow field that preserves essential structural motion cues. This process enables the transformation of large-scale image-mask pairs into image-flow-mask training pairs (as shown in Figure 1), dramatically addressing data scarcity while maintaining the structural information necessary for effective segmentation.

By training a simple encoder-decoder architecture with our synthesized data, we achieve new state-of-the-art performance on all public benchmark datasets, demonstrating a scalable solution to the data scarcity problem.

Our main contributions are summarized as follows:

- We propose DepthFlow, a novel data generation method that synthesizes optical flow from single images by converting estimated depth maps while preserving structural cues to transform image-mask pairs into large-scale image-flow-mask triplets.
- We demonstrate that VOS models can be trained effectively with synthetic flows that preserve structural information, achieving state-of-the-art performance using a simple encoder-decoder architecture.
- Our approach provides a scalable solution to the data scarcity problem by dramatically expanding available training data through image-to-flow conversion.

2. Related Work

Temporal reasoning. Many unsupervised VOS methods leverage temporal coherence across video frames to improve segmentation consistency. Early approaches like AGS [47] employ recurrent neural networks to model temporal dynamics while preserving spatial details. More recent methods explore various temporal modeling strategies: COSNet [24] uses co-attention modules for dense frame-pair comparisons, AGNN [46] treats frames as graph nodes with attentive propagation, and DFNet [56] models long-term correlations through discriminative feature learning. Reference-based methods include AD-Net [53], which uses initial frames as anchors for pairwise dependencies, and F2Net [22], which extends this with point heatmap estimation. Additionally, 3DC-Seg [25] and D²Conv3D [36] adopt 3D convolutions for explicit spatio-temporal modeling, while IMP [20] sequentially connects and propagates image-level predictions.

Multi-modality fusion. To address RGB ambiguities, two-stream architectures integrate optical flow with appearance information. Various fusion strategies have been proposed: MATNet [57] uses deeply interleaved encoders for hierarchical interactions, RTNet [35] employs reciprocal transformation networks, and FSNet [15] utilizes full-duplex mu-

tual propagation. Attention-based methods include AMC-Net [52] with co-attention gating and TransportNet [54] with optimal transport matching. HFAN [30] aligns features across multiple embedding layers, while SimulFlow [14] performs joint extraction at the embedding stage.

To improve robustness, some methods incorporate additional techniques. TMO [6] trains motion encoders that can leverage appearance features when flow quality is poor. OAST [40] and DATTT [23] employ test-time learning for inference refinement, while GFA [39] uses training augmentation to align train-test distributions. However, these methods are fundamentally limited by the scarcity of complete image-flow-mask training datasets.

Hybrid approaches. Recent methods combine temporal reasoning with multi-modal fusion to leverage both long-term consistency and short-term motion cues. PMN [18] maintains an external memory bank for continuously updating appearance and motion features, while GSA-Net [19] and DPA [7] inject global video properties using reference frames, providing the network with comprehensive knowledge of each video sequence.

3. Approach

3.1. Preliminaries

Conventional pipeline. Recent unsupervised VOS methods predominantly adopt two-stream architectures that leverage both RGB images I and optical flow maps F for feature extraction. Optical flows are typically calculated as:

$$F^i = \Phi(I^i, I^{i+1}), \quad (1)$$

where $\Phi(I_1, I_2)$ computes optical flow from source frame I_1 to target frame I_2 , and i denotes the frame index. For the final frame, the target frame is set to the preceding frame. Given I and F for each frame, the segmentation mask S is obtained as:

$$S = \Psi(I, F; w), \quad (2)$$

where Ψ represents the segmentation network and w its learnable parameters. This process operates per-frame, assuming short-term motion cues provide sufficient information for primary object detection.

Training data scarcity. While two-stream VOS architectures are effective, their performance is fundamentally constrained by the scarcity of complete training datasets containing image-flow-mask triplets. The most commonly used dataset, DAVIS 2016 [31] training set, contains only 30 training video sequences, which lacks the diversity required for robust network learning.

To mitigate this limitation, existing methods employ two primary strategies. The first involves using large-scale video segmentation datasets such as YouTube-VOS [51]

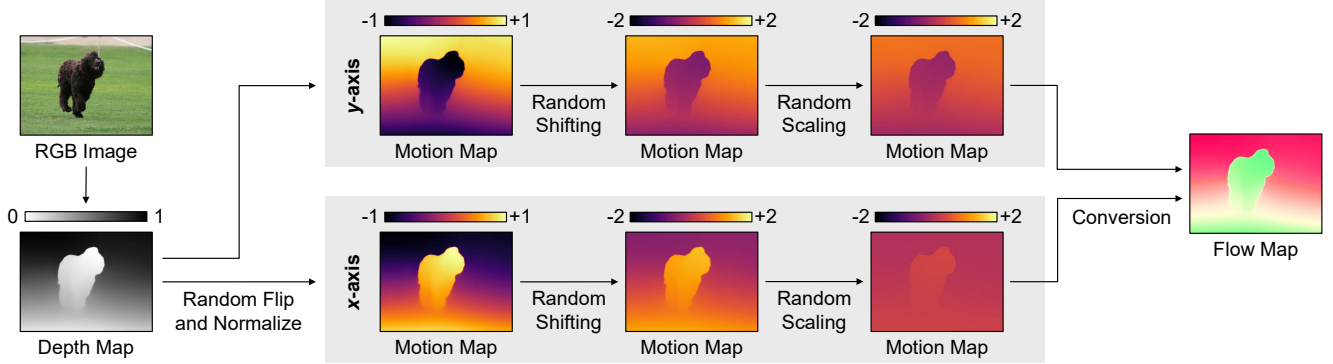


Figure 2. Illustration of our synthetic flow generation process from estimated depth maps.

and MOSE [9]. However, these datasets contain multiple annotated objects per frame, many of which are non-salient. Converting multi-label annotations to binary masks introduces training noise, making these datasets more suitable for pre-training than primary training. The second strategy utilizes image-level saliency datasets such as DUTS [44] or MSRA10K [3]. Since these datasets lack optical flow information, models cannot be trained in a complete setup, requiring subsequent fine-tuning on small complete datasets.

Both approaches are imperfect solutions that often lead to overfitting on limited complete datasets, ultimately hindering model generalization and performance.

Key observations. Our study is driven by two key observations about existing two-stream VOS approaches. First, most methods operate per-frame without needing to model long-term temporal relationships. This suggests that image-flow-mask pairs may suffice, eliminating the need for full video sequences. Second, VOS models rely on the structural information in flow maps, not their geometric precision, and this structure is highly correlated with depth. The primary objective is to capture structural motion cues that distinguish foreground from background. Therefore, synthetic flows that preserve essential structural information are sufficient for effective unsupervised VOS.

3.2. Depth-to-Flow Synthetic Data Generation

Building on our key observations that unsupervised VOS methods operate per-frame and rely on structural information in flow maps rather than geometric precision, we propose DepthFlow, a novel data generation method that synthesizes optical flow maps from single images. Our approach exploits the strong correlation between depth and flow structure: we first estimate a depth map from a source image and then convert it into a synthetic flow field that preserves essential structural cues. Figure 2 illustrates the complete pipeline.

Depth map estimation. We first estimate a depth map from each input image using a pre-trained monocular depth esti-

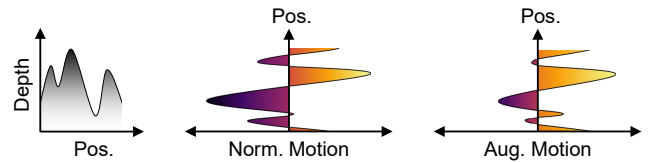


Figure 3. Visualized depth-to-flow conversion process. Augmented motion indicates the motion map after applying random value shifting and scaling.

mation model, DPT-Hybrid [34]. Let $f(\cdot)$ denote the depth estimation function. To ensure consistent value ranges across different images, we apply min-max normalization to obtain $D \in [0, 1]$:

$$D = \frac{f(I) - \min(f(I))}{\max(f(I)) - \min(f(I))}, \quad (3)$$

where the min and max operations are computed across all pixels in the depth map. This normalization provides a stable foundation for the subsequent flow synthesis process.

Motion map generation. Given the normalized depth map D , we convert it into synthetic optical flow patterns through a series of carefully designed transformations that simulate realistic motion characteristics. The generation process operates independently along the x and y axes, creating diverse two-channel optical flow maps while preserving the spatial relationships inherent in depth structures.

We first apply random depth reversal to create motion diversity with both positive and negative directions:

$$M_1 = 2r(1 - D) + 2(1 - r)D - 1, \quad r \stackrel{R}{\leftarrow} \{0, 1\}, \quad (4)$$

where r is a randomly selected binary value. This transformation generates diverse motion patterns by randomly determining the polarity of the depth-to-motion mapping, while normalizing values to the range $[-1, 1]$ to enable both positive and negative motion directions. Next, we introduce random value shifting to further enhance motion diversity:

$$M_2 = M_1 + s, \quad s \stackrel{R}{\leftarrow} [-1, 1]. \quad (5)$$

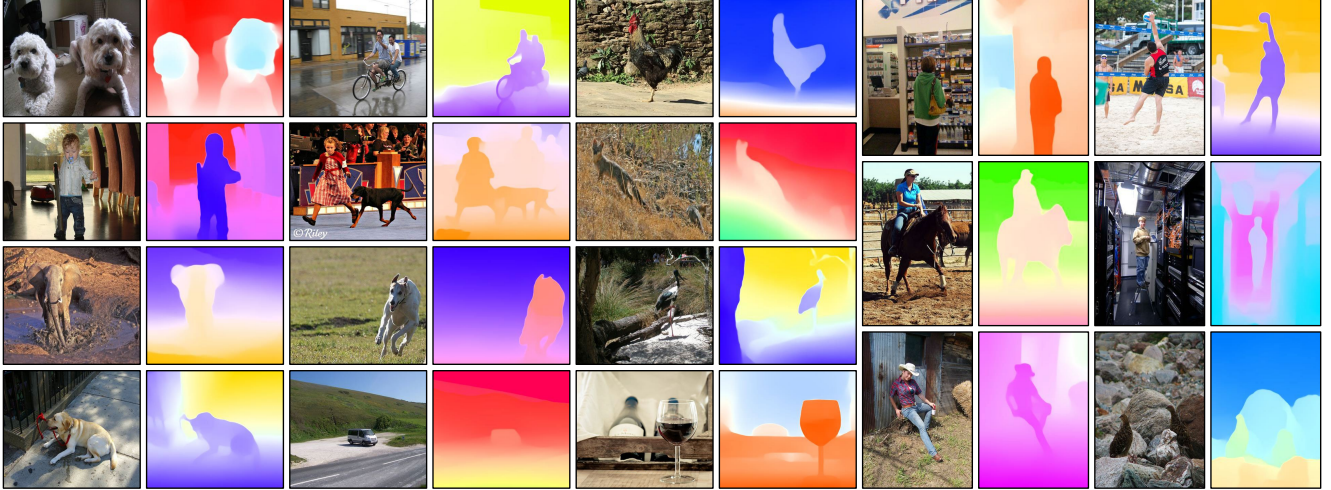


Figure 4. Representative image-flow pairs from our DUTSv2 dataset.

By adding random offsets s uniformly across all pixels, we shift the motion baseline to create additional directional variations, enabling comprehensive coverage of both positive and negative pixel displacements that characterize real optical flow patterns. Finally, we apply random value scaling to control motion magnitude and simulate varying flow intensities:

$$M_3 = \alpha \cdot M_2, \quad \alpha \stackrel{\mathbb{R}}{\leftarrow} [0, 1]. \quad (6)$$

This scaling operation modulates the optical flow magnitude from subtle to pronounced movements, reflecting the diverse range of motion intensities encountered in real video sequences. Figure 3 visualizes this motion map generation process, demonstrating how diverse synthetic optical flow patterns are systematically generated from a single depth map through these sequential transformations.

Flow map visualization. The resulting two-channel motion map $M_3 \in [-2, 2]$ requires normalization and conversion to RGB format for compatibility with standard optical flow processing pipelines. We first normalize the motion values by scaling the maximum absolute value in both horizontal and vertical components to 1:

$$M = \frac{M_3}{\max(\max(|M_3^x|), \max(|M_3^y|))}, \quad (7)$$

where M_3^x and M_3^y represent the horizontal and vertical components of the motion map, respectively. This normalization preserves relative motion patterns while standardizing the dynamic range for consistent processing. The normalized motion map is then converted to RGB format using the standard flow visualization protocol:

$$F = \text{UV2RGB}(M), \quad (8)$$

Table 1. Training data comparison showing the substantial increase in scale and diversity achieved by our synthetic data.

Dataset	#Triplets	#Visual Contexts
Real	2,079	30
Synthetic	15,572	15,572
Mixed	17,651	15,602

where UV2RGB represents the conventional mapping function that transforms two-channel motion vectors into three-channel RGB flow visualizations suitable for feature embedding in optical flow processing networks.

3.3. Large-Scale Dataset Construction

We apply our depth-to-flow synthetic data generation method to construct a comprehensive training dataset for two-stream VOS architectures. Using DUTS [44], a large-scale image-level SOD dataset containing 10,553 training and 5,019 testing image-mask pairs, as our foundation, we generate synthetic flow maps for all images in both splits. The resulting image-flow-mask triplets form our augmented dataset, referred to as DUTSv2, which provides over 15,000 complete training samples compared to the 30 video sequences available in DAVIS 2016 [31]. Figure 4 showcases representative image-flow pairs from DUTSv2, demonstrating the diversity and plausibility of our synthetic flows across various scene types and object categories.

Table 1 provides a quantitative comparison of training data scale and diversity between real and synthetic datasets. Here, visual diversity is defined as the number of distinct scenes or visual environments used during training. While real video dataset, DAVIS 2016 training set, contains multiple frames from the same 30 video sequences (resulting in 2,079 training pairs but only 30 distinct visual environ-

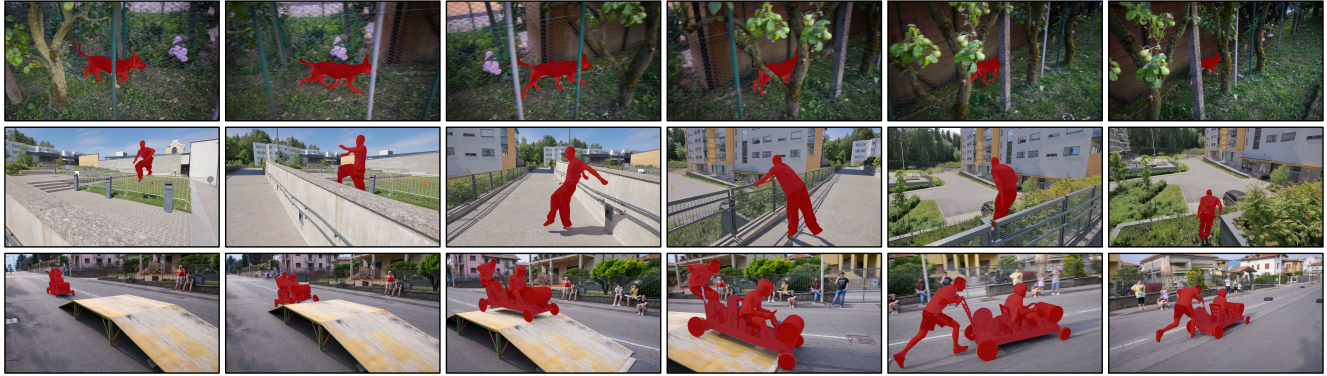


Figure 5. Qualitative results on the DAVIS 2016 validation set.

ments), our synthetic approach generates flows from individual images, providing 15,572 unique visual environments. This dramatic increase in visual diversity is crucial for network generalization, as it exposes the model to a much broader range of scenes, objects, and motion patterns than real video-based training. The mixed dataset combines both real and synthetic data, resulting in 17,651 total triplets spanning 15,602 distinct visual environments, representing over $500\times$ more visual diversity compared to real data alone.

For video datasets used in training and evaluation, optical flow maps are computed using RAFT [42] at original resolution to maintain data quality. Each video frame, consisting of an RGB image, optical flow map, and segmentation mask, is treated as an independent image-flow-mask triplet. This processing approach maintains consistency with the DUTSv2 structure and aligns with the per-frame processing paradigm adopted by modern unsupervised VOS methods, enabling seamless integration of both synthetic and real data during training.

3.4. Implementation Details

Network architecture. We adopt a simple encoder-decoder architecture similar to TMO [6] with two encoders processing RGB image and optical flow independently. Features from both encoders are fused at multiple layers through element-wise addition and decoded to produce segmentation masks. Following existing methods [4, 5], we incorporate CBAM [49] attention modules after each fusion step.

Network training. Our model is trained in an end-to-end manner using fully supervised learning with image-flow-mask triplets, learning to map input image-flow pairs directly to segmentation masks. We adopt a two-stage training protocol to provide comprehensive knowledge to the network. In the first stage, we pre-train the model using the YouTube-VOS 2018 [51] training set, merging all annotated objects into single binary masks as salient objects. In the second stage, we fine-tune using a combination of DAVIS

2016 training set and our DUTSv2 dataset with a mixing ratio of 1:3, ensuring the network benefits from both real video data and our large-scale synthetic dataset. For optimization, we employ cross-entropy loss and Adam [17] optimizer with learning rate $1e-5$. All training is conducted on two GeForce RTX TITAN GPUs with standard data augmentation techniques.

4. Experiments

We conduct extensive experiments to validate the effectiveness of our proposed approach. For unsupervised VOS, we evaluate on DAVIS 2016 [31] validation set, FBMS [27] test set, YouTube-Objects [33] dataset, and Long-Videos [21] dataset. For video SOD, we evaluate on DAVIS 2016 validation set, FBMS test set, DAVSOD [10] test set, and ViSal [45] dataset. We refer to our method as DepthFlow throughout this section for brevity.

4.1. Qualitative Results

Figure 5 showcases qualitative mask prediction results that demonstrate DepthFlow’s robustness in challenging scenarios. Despite severe occlusions, rapid camera motion, and complex background clutter, DepthFlow consistently segments primary objects with high accuracy. These results highlight the effectiveness of training with diverse synthetic flows to handle a broad spectrum of video complexities.

4.2. Quantitative Results

Unsupervised video object segmentation. Tables 2, 3, and 4 present quantitative comparisons between our method and existing state-of-the-art approaches on unsupervised VOS benchmarks. To ensure fair comparison, we specify the backbone architecture used in each method. The results demonstrate that constructing a robust training dataset is as crucial as designing sophisticated architectures. By improving only the training data through our depth-to-flow synthetic data generation, our method outperforms all existing approaches while maintaining efficient inference speeds.

Table 2. Quantitative evaluation on the DAVIS 2016 validation set and FBMS test set. OF and PP indicate the use of optical flow estimation model and post-processing technique, respectively. * denotes speed calculated on a single GeForce RTX 2080 Ti GPU.

Method	Publication	Backbone	Resolution	OF	PP	fps	DAVIS 2016			FBMS
							\mathcal{G}_M	\mathcal{J}_M	\mathcal{F}_M	\mathcal{J}_M
DFNet [56]	ECCV'20	DeepLabv3 [1]	-		✓	3.57	82.6	83.4	81.8	-
F2Net [22]	AAAI'21	DeepLabv3 [1]	473×473			10.0	83.7	83.1	84.4	77.5
RTNet [35]	CVPR'21	ResNet-101 [13]	384×672	✓	✓	-	85.2	85.6	84.7	-
FSNet [15]	ICCV'21	ResNet-50 [13]	352×352	✓	✓	12.5	83.3	83.4	83.1	-
TransportNet [54]	ICCV'21	ResNet-101 [13]	512×512	✓		12.5	84.8	84.5	85.0	78.7
AMC-Net [52]	ICCV'21	ResNet-101 [13]	384×384	✓	✓	17.5	84.6	84.5	84.6	76.5
D ² Conv3D [36]	WACV'22	ir-CSN-152 [43]	480×854			-	86.0	85.5	86.5	-
IMP [20]	AAAI'22	ResNet-50 [13]	-			1.79	85.6	84.5	86.7	77.5
HFAN [30]	ECCV'22	MiT-b2 [50]	512×512	✓		12.8*	87.5	86.8	88.2	-
PMN [18]	WACV'23	VGG-16 [38]	352×352	✓		41.3*	85.9	85.4	86.4	77.7
TMO [6]	WACV'23	ResNet-101 [13]	384×384	✓		43.2*	86.1	85.6	86.6	79.9
OAST [40]	ICCV'23	MobileViT3D [26]	384×640	✓		-	87.0	86.6	87.4	83.0
GFA [39]	AAAI'24	-	512×512	✓		-	88.2	87.4	88.9	82.4
GSA-Net [19]	CVPR'24	MiT-b2 [50]	512×512	✓		32.1*	88.2	87.4	89.0	82.3
DPA [7]	CVPR'24	VGG-16 [38]	512×512	✓		19.5*	87.6	86.8	88.4	83.4
DepthFlow		MiT-b2 [50]	512×512	✓		29.5*	88.5	88.0	89.0	84.7

Table 3. Quantitative evaluation on the YouTube-Objects dataset. Performance is reported with the \mathcal{J} mean.

Method	Backbone	Aero.	Bird	Boat	Car	Cat	Cow	Dog	Horse	Motor.	Train	Mean
COSNet [24]	DeepLabv3 [1]	81.1	75.7	71.3	77.6	66.5	69.8	76.8	67.4	67.7	46.8	70.5
AGNN [46]	DeepLabv3 [1]	71.1	75.9	70.7	78.1	67.9	69.7	77.4	67.3	68.3	47.8	70.8
HFAN [30]	MiT-b1 [50]	84.7	80.0	72.0	76.1	76.0	71.2	76.9	71.0	64.3	61.4	73.4
TMO [6]	ResNet-101 [13]	85.7	80.0	70.1	78.0	73.6	70.3	76.8	66.2	58.6	47.0	71.5
GFA [39]	-	87.2	85.5	74.7	82.9	80.4	72.0	79.6	67.8	61.3	55.8	74.7
GSA-Net [19]	MiT-b2 [50]	87.9	83.0	69.5	81.2	77.9	74.2	78.8	68.7	61.8	59.3	74.2
DPA [7]	VGG-16 [38]	87.5	85.6	70.1	77.7	81.2	69.0	81.8	61.9	62.1	51.3	73.7
DepthFlow	MiT-b2 [50]	86.9	86.2	74.5	82.5	80.8	71.8	80.8	66.1	55.9	63.3	75.1

This validates that depth-to-flow conversion preserves the structural patterns necessary for effective VOS learning.

Video salient object detection. Video SOD is closely related to unsupervised VOS and provides valuable evaluation of generalization capabilities. Table 5 presents results on video SOD benchmarks, demonstrating consistent performance improvements across multiple datasets. These results further validate that depth-to-flow conversion is sufficient for learning robust models, as the preserved structural patterns enable strong performance across related video understanding tasks. The consistent improvements highlight the broad applicability of our approach.

4.3. Analysis

Training protocol. Table 6 compares different training protocols: real (DAVIS 2016 [31] training set), synthetic (our DUTSv2 dataset), and mixed (both combined). Incorporating synthetic data significantly improves performance with and without pre-training. The gains are par-

Table 4. Quantitative evaluation on the Long-Videos dataset. SS and US denote semi-supervised and unsupervised, respectively.

Method	Backbone	Type	\mathcal{J}_M
STM [28]	ResNet-50 [13]	SS	79.1
AFB-URR [21]	ResNet-50 [13]	SS	82.7
AGNN [46]	DeepLabv3 [1]	US	68.3
HFAN [30]	MiT-b2 [50]	US	80.2
GSA-Net [19]	MiT-b2 [50]	US	80.6
DepthFlow	MiT-b2 [50]	US	81.1

ticularly substantial on FBMS [27], YouTube-Objects [33], and Long-Videos [21] datasets, which exhibit different domain characteristics from DAVIS. Remarkably, training exclusively on synthetic data outperforms real DAVIS training across these benchmarks, demonstrating that diverse synthetic training data provide more robust training signals than limited real video data.

Table 5. Quantitative evaluation on the DAVIS 2016 validation set, FBMS test set, DAVSOD test set, and ViSal dataset.

Method	DAVIS 2016			FBMS			DAVSOD			ViSal			Average		
	$S \uparrow$	$\mathcal{F} \uparrow$	$\mathcal{M} \downarrow$	$S \uparrow$	$\mathcal{F} \uparrow$	$\mathcal{M} \downarrow$	$S \uparrow$	$\mathcal{F} \uparrow$	$\mathcal{M} \downarrow$	$S \uparrow$	$\mathcal{F} \uparrow$	$\mathcal{M} \downarrow$	$S \uparrow$	$\mathcal{F} \uparrow$	$\mathcal{M} \downarrow$
SSAV [10]	89.3	86.1	2.8	87.9	86.5	4.0	72.4	60.3	9.2	94.3	93.9	2.0	86.0	81.7	4.5
AD-Net [53]	-	80.8	4.4	-	81.2	6.4	-	-	-	-	90.4	3.0	-	-	-
F ³ Net [48]	85.0	81.9	4.1	85.3	81.9	6.8	68.9	56.4	11.7	87.4	90.7	4.5	81.7	77.7	6.8
MINet [29]	86.1	83.5	3.9	84.9	81.7	6.7	70.4	58.2	10.3	90.3	91.1	4.1	82.9	78.6	6.3
GateNet [55]	86.9	84.6	3.6	85.7	83.2	6.5	70.1	57.8	10.4	92.1	92.8	3.9	83.7	79.6	6.1
PCSA [12]	90.2	88.0	2.2	86.6	83.1	4.1	74.1	65.5	8.6	94.6	94.0	1.7	86.4	82.7	4.2
3DC-Seg [25]	-	91.8	1.5	-	84.5	4.8	-	-	-	-	92.2	1.9	-	-	-
CASNet [16]	87.3	86.0	3.2	85.6	86.3	5.6	69.4	-	8.9	82.0	84.7	2.9	81.1	-	5.2
FSNet [15]	92.0	90.7	2.0	89.0	88.8	4.1	77.3	68.5	<u>7.2</u>	-	-	-	-	-	-
CFAM [2]	91.8	90.9	1.5	90.9	91.5	<u>2.6</u>	75.3	66.2	8.3	94.7	<u>95.1</u>	1.3	88.2	85.9	3.4
UFO [41]	91.8	90.6	1.5	89.1	88.8	3.1	-	-	-	95.9	<u>95.1</u>	1.3	-	-	-
DBSNet [11]	92.4	91.4	1.4	88.2	88.5	3.8	77.8	68.8	7.6	93.1	92.8	2.0	87.9	85.4	3.7
HFAN [30]	93.4	<u>92.9</u>	0.9	87.5	84.9	3.3	75.3	68.0	7.0	94.1	93.5	<u>1.1</u>	87.6	84.8	3.1
TMO [6]	92.8	92.0	0.9	88.6	88.2	3.1	76.7	70.8	<u>7.2</u>	94.2	94.7	1.0	88.1	86.4	3.1
OAST [40]	<u>93.5</u>	92.6	<u>1.1</u>	<u>91.7</u>	<u>91.9</u>	2.5	<u>78.6</u>	<u>71.2</u>	7.0	94.8	95.0	1.0	<u>89.7</u>	<u>87.7</u>	2.9
DepthFlow	94.6	94.1	<u>1.1</u>	92.2	92.0	2.7	80.2	72.7	7.0	<u>95.7</u>	96.3	1.3	90.7	88.8	<u>3.0</u>

Table 6. Ablation study on the training data setting. Pre. indicates the use of pre-training with large-scale video segmentation data.

Version	Pre.	Training	D	F	Y	L
I		Real	83.2	66.2	62.2	60.5
II		Synthetic	79.5	79.8	74.9	74.9
III		Mixed	87.6	82.7	72.5	77.2
IV	✓	-	82.2	81.7	73.3	68.3
V	✓	Real	87.7	81.8	72.8	73.2
VI	✓	Synthetic	85.8	83.4	76.5	82.0
VII	✓	Mixed	88.5	84.7	75.1	81.1

Table 7. Ablation study on the backbone network.

Backbone	fps	D	F	Y	L
MiT-b0	61.1	86.7	81.2	70.4	75.7
MiT-b1	45.5	87.3	81.8	73.5	77.9
MiT-b2	29.5	88.5	84.7	75.1	81.1

Backbone network. Table 7 compares various backbone architectures. Larger backbones achieve higher performance across all datasets at the cost of increased computational requirements. The consistent performance improvements with larger backbones validate the quality of our synthetic data, as poor-quality data would limit model scaling regardless of architecture capacity. We use MiT-b2 as the default backbone for all experiments.

Aligned comparison. To validate DepthFlow’s effectiveness, Table 8 presents direct comparisons with HFAN [30], which employs a similar two-stream pipeline and per-frame inference protocol. Our method consistently outperforms HFAN in both inference speed and segmentation accu-

Table 8. Aligned comparison on the DAVIS 2016 validation set. The speed is calculated on the same hardware.

Method	Backbone	fps	\mathcal{G}_M	\mathcal{J}_M	\mathcal{F}_M
HFAN [30]	MiT-b0	21.8	81.2	81.5	80.8
	MiT-b1	18.4	86.7	86.2	87.1
	MiT-b2	12.8	87.5	86.8	88.2
DepthFlow	MiT-b0	61.1	86.7	86.5	87.0
	MiT-b1	45.5	87.3	87.0	87.6
	MiT-b2	29.5	88.5	88.0	89.0

Table 9. Controlled experiment to evaluate model flexibility.

Method	Flow	D	F	Y	L
TMO [6]		80.0	80.0	73.1	67.7
	✓	86.1	79.9	71.5	72.5
DepthFlow		86.2	81.2	75.3	78.3
	✓	88.5	84.7	75.1	81.1

racy across all backbone variants. Notably, with smaller backbones where pre-trained knowledge is less leveraged, HFAN struggles to extract meaningful information from limited high-quality training data, leading to overfitting. These results demonstrate that well-designed training data can be more impactful than sophisticated network architectures, supporting our core contribution.

Model flexibility. While our method requires image-flow pairs for prediction, it can generate synthetic flows from individual video frames, enabling operation without real optical flows and effectively functioning as an image-level SOD model. To evaluate this flexibility, we compare with



Figure 6. Qualitative results on the general video cases.

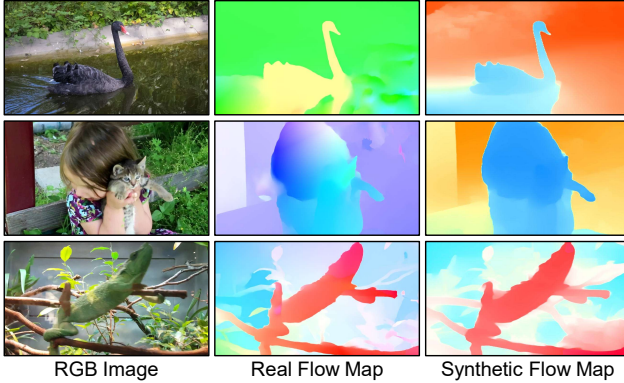


Figure 7. Visual comparison between real flow maps from flow estimation model and our generated flow maps.

TMO [6], which also provides motion-independent inference capability, as shown in Table 9. DepthFlow outperforms TMO across all benchmark datasets both with and without optical flow maps, demonstrating superior adaptability. Although using synthetic flows introduces minor performance variations compared to real flows, these differences remain negligible, confirming the robustness.

General video cases. Figure 6 presents results on general videos from the MOSE [9] validation set. Without any additional training or fine-tuning, the model trained under our setting consistently detects the salient objects, demonstrating strong generalization to real-world video scenarios.

Comparison to real flows. Figure 7 provides qualitative comparison between real optical flows (estimated using pre-trained models) and our synthetic flows (generated via depth-to-flow conversion) on DAVIS 2017 [32] dataset. While the synthetic flows may not capture geometrically precise motion, they exhibit plausible motion patterns that effectively distinguish foreground from background. Our depth-to-flow conversion preserves essential structural patterns, demonstrating that structural motion information is sufficient for robust VOS training.

Data distribution. In Figure 8, we extract features from both RGB images and flow maps using pre-trained encoders and visualize their distributions using t-SNE. The analysis reveals that features from our synthetic DUTSv2 dataset

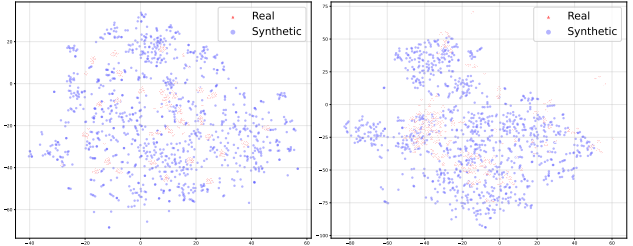


Figure 8. t-SNE comparison of feature distributions from real and synthetic datasets (left: RGB images, right: optical flow maps).

closely align with those from real DAVIS 2016 data in both modalities. Importantly, the synthetic data also fills under-represented regions in the feature space, effectively expanding the coverage of real data distributions. This demonstrates that our synthetic data generation approach not only maintains realistic feature characteristics but also provides enhanced diversity, supporting its effectiveness as a scalable training source for robust VOS models.

Limitations. DepthFlow relies on predicted depth maps to generate synthetic training data, making the quality of the training data dependent on the accuracy of depth estimation. Inaccuracies in depth prediction, especially in challenging scenes, can lead to suboptimal flow generation and affect downstream performance. While our current framework uses real optical flow during inference, a promising future direction is to investigate whether depth-to-flow simulation can also help compensate for low-quality or unreliable flow estimates at test time, potentially offering a more robust motion representation under adverse conditions.

5. Conclusion

Data scarcity remains a key bottleneck in unsupervised VOS. We propose a depth-to-flow synthetic data generation method that achieves state-of-the-art performance without complex architectures or heavy post-processing. Our findings demonstrate that synthetic flows, when preserving structural information, can effectively complement real training data, showing that high-quality data is as important as network design. This work provides a strong foundation for future synthetic data generation in video understanding.

References

- [1] Liang-Chieh Chen, George Papandreou, Florian Schroff, and Hartwig Adam. Rethinking atrous convolution for semantic image segmentation. *arXiv preprint arXiv:1706.05587*, 2017. [vi](#)
- [2] Yi-Wen Chen, Xiaojie Jin, Xiaohui Shen, and Ming-Hsuan Yang. Video salient object detection via contrastive features and attention modules. In *Proceedings of the IEEE/CVF winter conference on applications of computer vision*, pages 1320–1329, 2022. [vii](#)
- [3] Ming-Ming Cheng, Niloy J Mitra, Xiaolei Huang, Philip HS Torr, and Shi-Min Hu. Global contrast based salient region detection. *IEEE transactions on pattern analysis and machine intelligence*, 37(3):569–582, 2014. [i](#), [iii](#)
- [4] Suhwan Cho, Heansung Lee, Minjung Kim, Sungjun Jang, and Sangyoun Lee. Pixel-level bijective matching for video object segmentation. In *Proceedings of the IEEE/CVF Winter Conference on Applications of Computer Vision*, pages 129–138, 2022. [v](#)
- [5] Suhwan Cho, Heansung Lee, Minhyeok Lee, Chaewon Park, Sungjun Jang, Minjung Kim, and Sangyoun Lee. Tackling background distraction in video object segmentation. In *European Conference on Computer Vision*, pages 446–462. Springer, 2022. [v](#)
- [6] Suhwan Cho, Minhyeok Lee, Seunghoon Lee, Chaewon Park, Donghyeong Kim, and Sangyoun Lee. Treating motion as option to reduce motion dependency in unsupervised video object segmentation. In *Proceedings of the IEEE/CVF winter conference on applications of computer vision*, pages 5140–5149, 2023. [ii](#), [v](#), [vi](#), [vii](#), [viii](#)
- [7] Suhwan Cho, Minhyeok Lee, Seunghoon Lee, Dogyoon Lee, Heeseung Choi, Ig-Jae Kim, and Sangyoun Lee. Dual prototype attention for unsupervised video object segmentation. In *Proceedings of the IEEE/CVF Conference on Computer Vision and Pattern Recognition*, pages 19238–19247, 2024. [ii](#), [vi](#)
- [8] Henghui Ding, Chang Liu, Shuting He, Xudong Jiang, and Chen Change Loy. Mevis: A large-scale benchmark for video segmentation with motion expressions. In *Proceedings of the IEEE/CVF International Conference on Computer Vision*, pages 2694–2703, 2023. [i](#)
- [9] Henghui Ding, Chang Liu, Shuting He, Xudong Jiang, Philip HS Torr, and Song Bai. Mose: A new dataset for video object segmentation in complex scenes. In *Proceedings of the IEEE/CVF international conference on computer vision*, pages 20224–20234, 2023. [i](#), [iii](#), [viii](#)
- [10] Deng-Ping Fan, Wenguan Wang, Ming-Ming Cheng, and Jianbing Shen. Shifting more attention to video salient object detection. In *Proceedings of the IEEE/CVF conference on computer vision and pattern recognition*, pages 8554–8564, 2019. [v](#), [vii](#)
- [11] Jiaqing Fan, Tiankang Su, Kaihua Zhang, and Qingshan Liu. Bidirectionally learning dense spatio-temporal feature propagation network for unsupervised video object segmentation. In *Proceedings of the 30th ACM International Conference on Multimedia*, pages 3646–3655, 2022. [vii](#)
- [12] Yuchao Gu, Lijuan Wang, Ziqin Wang, Yun Liu, Ming-Ming Cheng, and Shao-Ping Lu. Pyramid constrained self-attention network for fast video salient object detection. In *Proceedings of the AAAI conference on artificial intelligence*, pages 10869–10876, 2020. [vii](#)
- [13] Kaiming He, Xiangyu Zhang, Shaoqing Ren, and Jian Sun. Deep residual learning for image recognition. In *Proceedings of the IEEE conference on computer vision and pattern recognition*, pages 770–778, 2016. [vi](#)
- [14] Lingyi Hong, Wei Zhang, Shuyong Gao, Hong Lu, and Wen-Qiang Zhang. Simulflow: Simultaneously extracting feature and identifying target for unsupervised video object segmentation. In *Proceedings of the 31st ACM International Conference on Multimedia*, pages 7481–7490, 2023. [ii](#)
- [15] Ge-Peng Ji, Keren Fu, Zhe Wu, Deng-Ping Fan, Jianbing Shen, and Ling Shao. Full-duplex strategy for video object segmentation. In *Proceedings of the IEEE/CVF international conference on computer vision*, pages 4922–4933, 2021. [ii](#), [vi](#), [vii](#)
- [16] Yuzhu Ji, Haijun Zhang, Zequn Jie, Lin Ma, and QM Jonathan Wu. Casnet: A cross-attention siamese network for video salient object detection. *IEEE transactions on neural networks and learning systems*, 32(6):2676–2690, 2020. [vii](#)
- [17] Diederik P Kingma and Jimmy Ba. Adam: A method for stochastic optimization. *arXiv preprint arXiv:1412.6980*, 2014. [v](#)
- [18] Minhyeok Lee, Suhwan Cho, Seunghoon Lee, Chaewon Park, and Sangyoun Lee. Unsupervised video object segmentation via prototype memory network. In *Proceedings of the IEEE/CVF winter conference on applications of computer vision*, pages 5924–5934, 2023. [ii](#), [vi](#)
- [19] Minhyeok Lee, Suhwan Cho, Dogyoon Lee, Chaewon Park, Jungho Lee, and Sangyoun Lee. Guided slot attention for unsupervised video object segmentation. In *Proceedings of the IEEE/CVF Conference on Computer Vision and Pattern Recognition*, pages 3807–3816, 2024. [ii](#), [vi](#)
- [20] Youngjo Lee, Hongje Seong, and Euntai Kim. Iteratively selecting an easy reference frame makes unsupervised video object segmentation easier. In *Proceedings of the AAAI Conference on Artificial Intelligence*, pages 1245–1253, 2022. [ii](#), [vi](#)
- [21] Yongqing Liang, Xin Li, Navid Jafari, and Jim Chen. Video object segmentation with adaptive feature bank and uncertain-region refinement. *Advances in Neural Information Processing Systems*, 33:3430–3441, 2020. [v](#), [vi](#)
- [22] Daizong Liu, Dongdong Yu, Changhu Wang, and Pan Zhou. F2net: Learning to focus on the foreground for unsupervised video object segmentation. In *Proceedings of the AAAI conference on artificial intelligence*, pages 2109–2117, 2021. [ii](#), [vi](#)
- [23] Weihuang Liu, Xi Shen, Haolun Li, Xiuli Bi, Bo Liu, Chi-Man Pun, and Xiaodong Cun. Depth-aware test-time training for zero-shot video object segmentation. In *Proceedings of the IEEE/CVF Conference on Computer Vision and Pattern Recognition*, pages 19218–19227, 2024. [ii](#)
- [24] Xiankai Lu, Wenguan Wang, Chao Ma, Jianbing Shen, Ling Shao, and Fatih Porikli. See more, know more: Unsuper-

- vised video object segmentation with co-attention siamese networks. In *Proceedings of the IEEE/CVF conference on computer vision and pattern recognition*, pages 3623–3632, 2019. [ii](#), [vi](#)
- [25] Sabarinath Mahadevan, Ali Athar, Aljoša Ošep, Sebastian Hennen, Laura Leal-Taixé, and Bastian Leibe. Making a case for 3d convolutions for object segmentation in videos. *arXiv preprint arXiv:2008.11516*, 2020. [ii](#), [vii](#)
- [26] Sachin Mehta and Mohammad Rastegari. Mobilevit: lightweight, general-purpose, and mobile-friendly vision transformer. *arXiv preprint arXiv:2110.02178*, 2021. [vi](#)
- [27] Peter Ochs, Jitendra Malik, and Thomas Brox. Segmentation of moving objects by long term video analysis. *IEEE transactions on pattern analysis and machine intelligence*, 36(6): 1187–1200, 2013. [v](#), [vi](#)
- [28] Seoung Wug Oh, Joon-Young Lee, Ning Xu, and Seon Joo Kim. Video object segmentation using space-time memory networks. In *Proceedings of the IEEE/CVF international conference on computer vision*, pages 9226–9235, 2019. [vi](#)
- [29] Youwei Pang, Xiaoqi Zhao, Lihe Zhang, and Huchuan Lu. Multi-scale interactive network for salient object detection. In *Proceedings of the IEEE/CVF conference on computer vision and pattern recognition*, pages 9413–9422, 2020. [vii](#)
- [30] Gensheng Pei, Fumin Shen, Yazhou Yao, Guo-Sen Xie, Zhenmin Tang, and Jinhui Tang. Hierarchical feature alignment network for unsupervised video object segmentation. In *European Conference on Computer Vision*, pages 596–613. Springer, 2022. [ii](#), [vi](#), [vii](#)
- [31] Federico Perazzi, Jordi Pont-Tuset, Brian McWilliams, Luc Van Gool, Markus Gross, and Alexander Sorkine-Hornung. A benchmark dataset and evaluation methodology for video object segmentation. In *Proceedings of the IEEE conference on computer vision and pattern recognition*, pages 724–732, 2016. [ii](#), [iv](#), [v](#), [vi](#)
- [32] Jordi Pont-Tuset, Federico Perazzi, Sergi Caelles, Pablo Arbeláez, Alexander Sorkine-Hornung, and Luc Van Gool. The 2017 davis challenge on video object segmentation. *arXiv:1704.00675*, 2017. [viii](#)
- [33] Alessandro Prest, Christian Leistner, Javier Civera, Cordelia Schmid, and Vittorio Ferrari. Learning object class detectors from weakly annotated video. In *2012 IEEE Conference on computer vision and pattern recognition*, pages 3282–3289. IEEE, 2012. [v](#), [vi](#)
- [34] René Ranftl, Alexey Bochkovskiy, and Vladlen Koltun. Vision transformers for dense prediction. In *Proceedings of the IEEE/CVF international conference on computer vision*, pages 12179–12188, 2021. [iii](#)
- [35] Sucheng Ren, Wenxi Liu, Yongtuo Liu, Haoxin Chen, Guoqiang Han, and Shengfeng He. Reciprocal transformations for unsupervised video object segmentation. In *Proceedings of the IEEE/CVF conference on computer vision and pattern recognition*, pages 15455–15464, 2021. [ii](#), [vi](#)
- [36] Christian Schmidt, Ali Athar, Sabarinath Mahadevan, and Bastian Leibe. D2conv3d: Dynamic dilated convolutions for object segmentation in videos. In *Proceedings of the IEEE/CVF winter conference on applications of computer vision*, pages 1200–1209, 2022. [ii](#), [vi](#)
- [37] Jianping Shi, Qiong Yan, Li Xu, and Jiaya Jia. Hierarchical image saliency detection on extended cssd. *IEEE transactions on pattern analysis and machine intelligence*, 38(4): 717–729, 2015. [i](#)
- [38] Karen Simonyan and Andrew Zisserman. Very deep convolutional networks for large-scale image recognition. *arXiv preprint arXiv:1409.1556*, 2014. [vi](#)
- [39] Huihui Song, Tiankang Su, Yuhui Zheng, Kaihua Zhang, Bo Liu, and Dong Liu. Generalizable fourier augmentation for unsupervised video object segmentation. In *Proceedings of the AAAI conference on artificial intelligence*, pages 4918–4924, 2024. [ii](#), [vi](#)
- [40] Tiankang Su, Huihui Song, Dong Liu, Bo Liu, and Qingshan Liu. Unsupervised video object segmentation with online adversarial self-tuning. In *Proceedings of the IEEE/CVF International Conference on Computer Vision*, pages 688–698, 2023. [ii](#), [vi](#), [vii](#)
- [41] Yukun Su, Jingliang Deng, Ruizhou Sun, Guosheng Lin, Hanjing Su, and Qingyao Wu. A unified transformer framework for group-based segmentation: Co-segmentation, co-saliency detection and video salient object detection. *IEEE Transactions on Multimedia*, 26:313–325, 2023. [vii](#)
- [42] Zachary Teed and Jia Deng. Raft: Recurrent all-pairs field transforms for optical flow. In *Computer Vision—ECCV 2020: 16th European Conference, Glasgow, UK, August 23–28, 2020, Proceedings, Part II 16*, pages 402–419. Springer, 2020. [v](#)
- [43] Du Tran, Heng Wang, Lorenzo Torresani, and Matt Feiszli. Video classification with channel-separated convolutional networks. In *Proceedings of the IEEE/CVF international conference on computer vision*, pages 5552–5561, 2019. [vi](#)
- [44] Lijun Wang, Huchuan Lu, Yifan Wang, Mengyang Feng, Dong Wang, Baocai Yin, and Xiang Ruan. Learning to detect salient objects with image-level supervision. In *CVPR*, 2017. [i](#), [iii](#), [iv](#)
- [45] Wenguan Wang, Jianbing Shen, and Ling Shao. Consistent video saliency using local gradient flow optimization and global refinement. *IEEE Transactions on Image Processing*, 24(11):4185–4196, 2015. [v](#)
- [46] Wenguan Wang, Xiankai Lu, Jianbing Shen, David J Crandall, and Ling Shao. Zero-shot video object segmentation via attentive graph neural networks. In *Proceedings of the IEEE/CVF international conference on computer vision*, pages 9236–9245, 2019. [ii](#), [vi](#)
- [47] Wenguan Wang, Hongmei Song, Shuyang Zhao, Jianbing Shen, Sanyuan Zhao, Steven CH Hoi, and Haibin Ling. Learning unsupervised video object segmentation through visual attention. In *Proceedings of the IEEE/CVF conference on computer vision and pattern recognition*, pages 3064–3074, 2019. [ii](#)
- [48] Jun Wei, Shuhui Wang, and Qingming Huang. F³net: fusion, feedback and focus for salient object detection. In *Proceedings of the AAAI conference on artificial intelligence*, pages 12321–12328, 2020. [vii](#)
- [49] Sanghyun Woo, Jongchan Park, Joon-Young Lee, and In So Kweon. Cbam: Convolutional block attention module. In

Proceedings of the European conference on computer vision (ECCV), pages 3–19, 2018. [v](#)

- [50] Enze Xie, Wenhai Wang, Zhiding Yu, Anima Anandkumar, Jose M Alvarez, and Ping Luo. Segformer: Simple and efficient design for semantic segmentation with transformers. *Advances in Neural Information Processing Systems*, 34:12077–12090, 2021. [vi](#)
- [51] Ning Xu, Linjie Yang, Yuchen Fan, Dingcheng Yue, Yuchen Liang, Jianchao Yang, and Thomas Huang. Youtube-vos: A large-scale video object segmentation benchmark. *arXiv preprint arXiv:1809.03327*, 2018. [i](#), [ii](#), [v](#)
- [52] Shu Yang, Lu Zhang, Jinqing Qi, Huchuan Lu, Shuo Wang, and Xiaoxing Zhang. Learning motion-appearance co-attention for zero-shot video object segmentation. In *Proceedings of the IEEE/CVF international conference on computer vision*, pages 1564–1573, 2021. [ii](#), [vi](#)
- [53] Zhao Yang, Qiang Wang, Luca Bertinetto, Weiming Hu, Song Bai, and Philip HS Torr. Anchor diffusion for unsupervised video object segmentation. In *Proceedings of the IEEE/CVF international conference on computer vision*, pages 931–940, 2019. [ii](#), [vii](#)
- [54] Kaihua Zhang, Zicheng Zhao, Dong Liu, Qingshan Liu, and Bo Liu. Deep transport network for unsupervised video object segmentation. In *Proceedings of the IEEE/CVF international conference on computer vision*, pages 8781–8790, 2021. [ii](#), [vi](#)
- [55] Xiaoqi Zhao, Youwei Pang, Lihe Zhang, Huchuan Lu, and Lei Zhang. Suppress and balance: A simple gated network for salient object detection. In *Computer Vision–ECCV 2020: 16th European Conference, Glasgow, UK, August 23–28, 2020, Proceedings, Part II 16*, pages 35–51. Springer, 2020. [vii](#)
- [56] Mingmin Zhen, Shiwei Li, Lei Zhou, Jiayang Shang, Haoan Feng, Tian Fang, and Long Quan. Learning discriminative feature with crf for unsupervised video object segmentation. In *Computer Vision–ECCV 2020: 16th European Conference, Glasgow, UK, August 23–28, 2020, Proceedings, Part XXVII 16*, pages 445–462. Springer, 2020. [ii](#), [vi](#)
- [57] Tianfei Zhou, Shunzhou Wang, Yi Zhou, Yazhou Yao, Jianwu Li, and Ling Shao. Motion-attentive transition for zero-shot video object segmentation. In *Proceedings of the AAAI conference on artificial intelligence*, pages 13066–13073, 2020. [ii](#)